SMEI Observations in the STEREO Era

Bernard V. Jackson*, Andrew Buffington**, P. Paul Hick***, Mario M. Bisi****,
and Elizabeth A. Jensen*****
Center for Astrophysics and Space Sciences, University of California, San Diego

ABSTRACT

White-light Thomson scattering observations from the Solar Mass Ejection Imager (SMEI) have recorded the inner heliospheric response to many CMEs. Some of these are also observed from the LASCO instrumentation and, most recently, the STEREO spacecraft. Here, we detail several CME events in SMEI observations that have also been observed by the LASCO instrumentation and STEREO spacecrafts. We show how SMEI is able to measure CME events from their first observations as close as 20° from the solar disk until they fade away in the SMEI 180° field of view. We employ a 3D reconstruction technique that provides perspective views as observed from Earth, from outward-flowing solar wind. This is accomplished by iteratively fitting the parameters of a kinematic solar wind density model to the SMEI white-light observations and, where possible, including interplanetary scintillation (IPS) velocity data. This 3D modeling technique enables separating the true heliospheric response in SMEI from background noise, and reconstructing the 3D heliospheric structure as a function of time. These reconstructions allow both separation of CME structure from other nearby heliospheric features and a determination of CME mass. Comparisons with LASCO and STEREO images for individual CMEs or portions of them allow a detailed view of changes to the CME shape and mass as they propagate outward.

Keywords: Coronal mass ejections, CME, corotating region interactions, CIR, tomography, 3D reconstructions

1. INTRODUCTION

The Solar Mass Ejection Imager (SMEI)[1,2] was launched on 6 January 2003. The instrument (Figure 1a) consists of three baffled cameras whose 3°×60° fields of view are aligned in the long dimension to achieve a combined ~160° wide field of view that scans most of the sky every 102-minute orbit (Figure 1b). The cameras are designed to view the heliosphere in Thomson scattered light at one-degree spatial resolution. Four-second exposure CCD camera data frames (Figure 2a; approximately 4500 per orbit)) are combined into a global mosaic sky map (Figure2b).

For the bulk of the data (in "science mode" with CCD pixels combined into 4×4 pixel averages) from camera 1 and 2 the angular resolution in the CCD image frames is ~0.2°. Camera 3 (which views closest to the Sun) usually operates in 2×2 mode and thus has a twice finer angular angular resolution. These images are stored and regularly telemetered to the ground employing a lossless Rice compression algorithm. Currently, SMEI returns about three gigabytes of data each day. The design specification for SMEI states that the SMEI instrument will provide a 0.1% photometric result in one square degree of sky at an elongation of 90º from the Sun in a single orbital sky map. This will provide a signal to noise of about 10% for dense heliospheric structures at this elongation[2]. We have found that at locations in the sky map when there is little contamination from high energy particle fluxes and no aurora light, that SMEI exceeds this specification by about a factor of two[3].

The overall SMEI design has progressed over a period of nearly two decades[1-2,4-8]. SMEI is currently the best design we know for operation near Earth on a spacecraft not specifically designed for the instrument, and where the Moon and stray light from spacecraft bus appendages thus have the potential to overwhelm the faint brightness signal from heliospheric electrons.

Solar Physics and Space Weather Instrumentation II, edited by Silvano Fineschi, Rodney A. Viereck
Proc. of SPIE Vol. 6689, 66890G, (2007) · 0277-786X/07/$18 · doi: 10.1117/12.734870

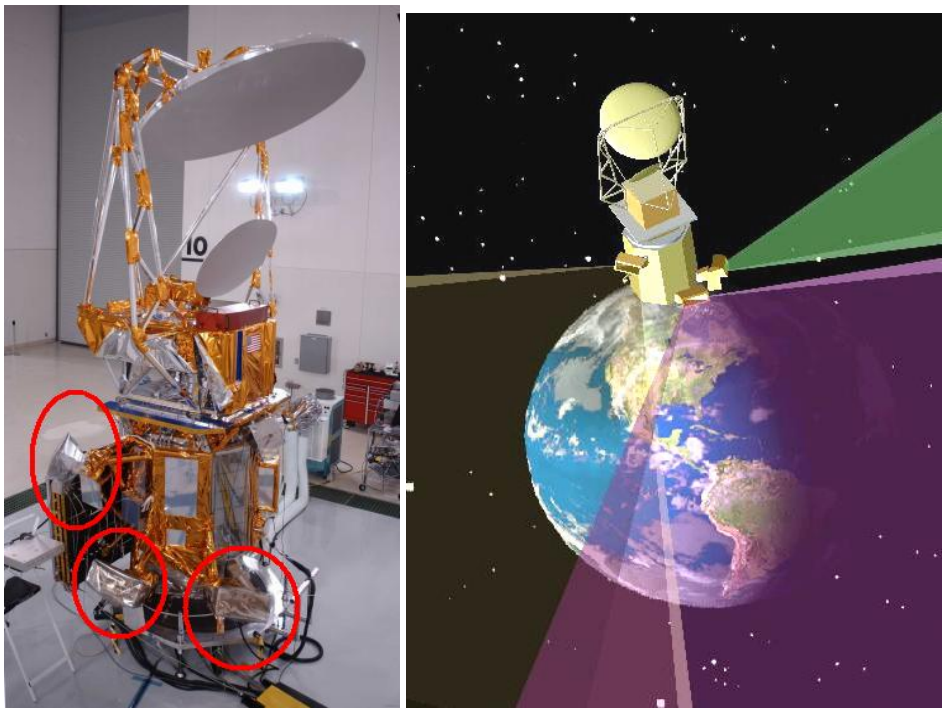

(a) **(b)**

Figure 1. (a) The Coriolis spacecraft with the Solar Mass Ejection Imager (SMEI) instrument and the *Windsat* antenna prior to launch from Vandenberg AFB. The three SMEI camera baffles (circled) are seen on the lower portion of the spacecraft. (**b)** SMEI in its polar orbit at 840 km with an orbital inclination of 98°. SMEI looks away from the Earth at 30° from the local horizontal to avoid sunlight reflected from the Earth and from the *Windsat* antenna. The combined fields of view of the three cameras (shown as shaded cones) cover nearly all of the sky.

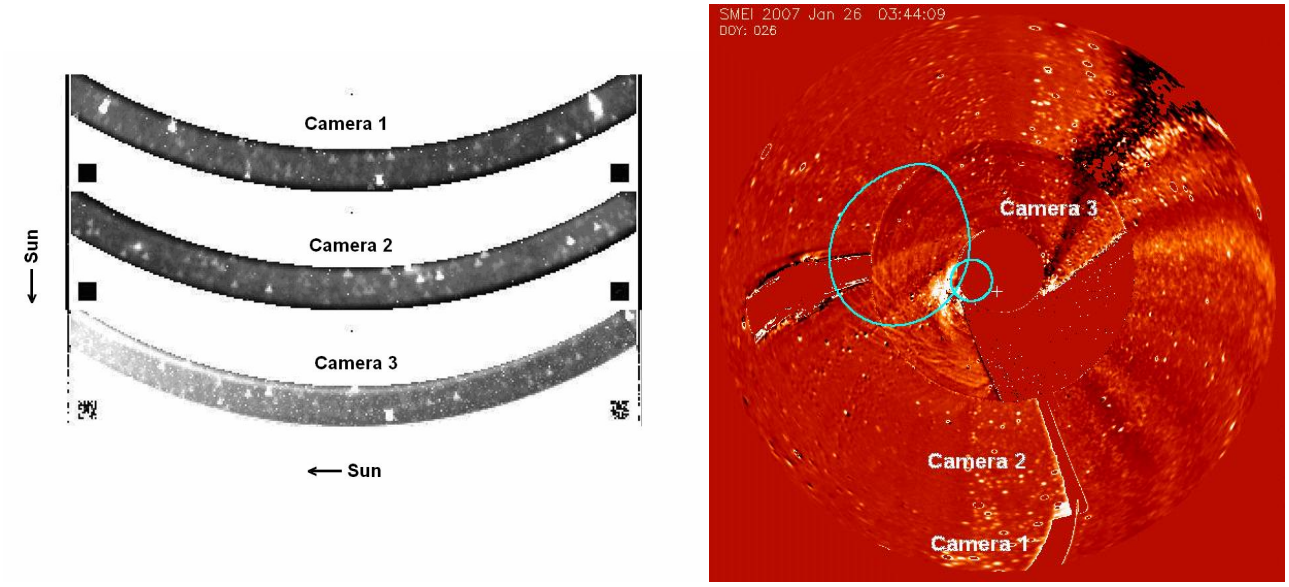

(a) **(b)**

Figure 2. (a) 3°×60° image frames from each of the three SMEI cameras. Camera 1 (top) views farthest from the Sun; camera 3 (bottom) closest, with the Sun towards the left in each frame. **(b)** Fisheye orbit-by-orbit difference projection of the sky to ~140º elongation built as a composite from SMEI data frames over a 102-minute orbit around Earth. Blank regions were excluded because they were not accessible to the cameras during the orbit, and were too close to the Sun and thus too bright, or contaminated by high-energy particle enhancements or the moon. See: **http://smei.ucsd.edu/**, and other links for more images and a SMEI archive of orbit by orbit difference maps. The Sun is in the center of the image marked as a cross. The fields of view of the STEREO "A" HI-1 (inner smaller region) and HI-2 (outer larger region) instruments are superimposed on the image and cover a fraction of SMEI's coverage.

The Solar Terrestrial Relations Observatory (STEREO) spacecraft[9] were launched on 26 October 2006. The STEREO spacecraft include *in situ* measurements of heliospheric protons from the PLAsma and SupraThermal Ion Composition (PLASTIC) instruments[10], and magnetic fields from the *In situ* Measurements of Particles and CME Transients

(IMPACT) instruments[11], as well as remote-sensing observations of Thomson-scattered light using a set of coronagraph-type systems (COR-1, COR-2, and HI-1, HI-2) as a portion of the instruments termed the Sun-Earth Connection and Heliospheric Investigation (SECCHI) instrument suite[12-14]. These latter instruments view the corona in a nearly continuous band along the ecliptic from the solar surface to slightly greater than 90º elongation (angular distance) from the Sun (see Figure 2b).

The joint NASA-European Space Agency (ESA) Ulysses mission[15], conceived to study the 3D heliosphere, has in August 2007 made its third close pass of the Sun in a non-ecliptic orbit. The ten experiments on board include the plasma Solar Wind thermal ion and electrons distributions instrument (SWOOPS)[16], and the Vector magnetometer (VHM/FGM) instrument[17] that measures heliospheric magnetic fields. The Ulysses spacecraft orbits as close to the Sun as 1.4 AU, and is well within the SMEI field of view during its close pass.

Observation of comet-tail aberration is the oldest of the remote-sensing heliospheric measurements[18]. Another source of heliospheric remote sensing information that operates in the present era includes the ground-based interplanetary scintillation (IPS) radio arrays that measure small-scale density irregularities in the interplanetary medium using meter-wavelength intensity variations from point radio sources. These data have long been used to measure small-scale(~150 km) heliospheric density variations along the line of sight to a distant compact radio source[19-21]. IPS observations prior to the Ulysses spacecraft polar passes were able to show that there are high speed solar winds over the solar poles at solar minimum[22].

There have been numerous attempts to reconstruct coronal structures in the corona and heliosphere in three dimensions (3D). The analysis of remote sensing data has primarily dealt with the reconstruction of coronal and heliospheric data using rotation as a means to reproduce structure. These techniques fail as solar wind outflow and non-stationary processes become more dominant. This has led to, or even demanded, observations of the transient structure and the implementation of observations to show heliospheric evolution such as from the Ulysses and STEREO spacecraft. The techniques to view structures in 3D, reviewed in Section 2, have been motivated by attempts to determine heliospheric structure morphology in order to determine their physics, their dynamics, and most recently to forecast their arrival at Earth using remote sensing techniques.

Section 2 gives a brief background of the motivation behind the heliospheric remote-sensing analyses and 3D reconstruction analyses. These include the SMEI and SECCHI remote-sensing instruments as well as interplanetary scintillation (IPS) observations data that are used to augment the UCSD SMEI remote sensing analysis and map heliospheric structures in 3D. Section 3 describes some of the new SMEI results. We conclude in Section 4.

2. HELIOSPHERIC REMOTE SENSING AND 3D RECONSTRUCTION

IPS and Thomson-scattering remote sensing observations provide one of very few means of observing structures in the solar wind located between the immediate solar environment (as observed by coronagraphs) and 1 AU (as observed by near-Earth *in situ* instruments). These remote sensing data probe the global extent of the solar wind over a large range of solar elongations. They also extend across the high-latitude regions (the solar poles), difficult of access by other means. Previous UCSD work has extensively employed these heliospheric remote sensing observations to study the physics of structures in the solar wind as they move out into the heliosphere.

The first sustained heliospheric remote-sensing measurements, IPS observations from the Cambridge, UK, array[19], generally showed structures that can be classified either as corotating or as detached from the Sun[20,23,24]. We have developed 3D techniques to analyze these[9,10,24,25]. In collaboration with colleagues at the Solar-Terrestrial Environment Laboratory (STELab), Nagoya University, Japan[25], UCSD currently operates a real-time, web-based system that forecasts solar wind conditions near Earth (see **http://ips.ucsd.edu/**). These data are used to interpolate 3D solar wind plasma and velocities at all the inner planets, and at the Ulysses spacecraft (see **http://ips.ucsd.edu/index_ss.html**).

The Thomson-scattering SMEI and SECCHI remote-sensing observations have obvious potential for studying propagation and evolution of heliospheric structures as they interact with each other and the ambient solar wind. However, as with coronagraph and IPS data, interpretation is complicated because each observation is a line-of-sight integration. Apparent brightness distribution and "plane-of-the-sky" motion depend on an *a priori* unknown 3D distribution of outward moving solar wind material at uncertain locations relative to Sun and Earth.

One can resolve the line-of-sight ambiguity by assuming the structures are all located in the plane of the sky. This provides useful information about persistent (corotating) solar wind structures[22,26]. However, when a transient structure such as a heliospheric response to a CME is followed across a wide range of solar elongations (as from the SMEI and the SECCHI instruments), the plane-of-the-sky assumption cannot remain correct over the whole elongation of the observations. In addition, the structure in general extends along a significant portion of the line of sight at all times, casting further doubt on this plane-of-the-sky assumption.

These considerations led us to develop an analysis tool that directly addresses the line-of-sight problem. It explicitly takes into account the 3D extent of heliospheric structures including the fact that the contribution is dominated by material closest to the Sun, but without explicit assumptions about the distribution of velocity and density along these lines of sight. Thus, it reconstructs 3D solar wind structures from remote sensing data gathered at a single location, as with SMEI. This technique is necessary to tap the full heliospheric-imager and IPS potential, and enable it as a predictive tool for space weather purposes.

This analysis is a general methodology to use views of a structure from many different perspectives to reconstruct its 3D shape. Usually, heliospheric remote-sensing observations are available from only a single viewing location, *i.e.*, from Earth. Perspective information in this case comes from solar rotation and outflow in the solar wind. In the first of these types of analyses using differing perspective views to reconstruct heliospheric structures, the assumption was used that structures change little except for corotation within one solar rotation. In this case rotation alone yields sufficient information for reconstruction of the quiet corona[27-39] and the corotating solar wind.

However, transients such as CMEs evolve on much shorter time scales, hours to days. For observations covering a wide range of solar elongations, heliospheric structures are seen from widely different directions as they move past Earth. This feature, essentially absent in coronagraph data, allows 3D reconstruction using heliospheric data such as from SMEI, for time-dependent reconstruction of transient structures, by fitting a solar wind model to the outward-flowing plasma structures [40-45].

Presently, our 3D reconstruction incorporates a purely kinematic solar wind model. Given the velocity and density of an inner boundary (the "source surface"), a fully 3D solar wind model best fitting the observations follows, by assuming radial outflow and enforcing conservation of mass and mass flux[37,43,44]. Best fit is achieved iteratively: if the 3D solar wind at large solar distances does not match the overall observations, the source surface values are changed to reduce the deviations to a desired small value.

We have employed this technique to successfully analyze CME-associated structures using IPS and SMEI Thomson scattering observations. Thomson scattering brightness measures density much closer than the IPS "*g*-level" density proxy in the IPS 3D reconstructions. Thus, SMEI 3D reconstruction analyses[44] are free of using the IPS *g*-level proxy for density, and of course much more abundant in the number of lines of sight than current IPS observations. However, the Thomson-scattering 3D reconstruction analysis must take into account, in addition to the observed time-varying signal, that there is an unknown steady background component caused by the ambient heliospheric brightness, and potentially an unknown zodiacal light residual brightness not removed in the long-term zodiacal light average. An estimate of this residual brightness is modeled by relating model densities to *in situ* observations, near Earth. A mean of *in situ* densities over time for several weeks allows a solar wind ambient to be determined relative to the shorter term variations (on the order of hours to days) observed as structures flow past the Earth. Brightness relative to this ambient that is either positive or negative can be reconstructed in the time-dependent reconstruction technique as outward-flowing solar wind structure.

SMEI cameras are currently being calibrated using known G-star brightness, and this calibration is currently estimated to be accurate to ~5% for all three SMEI cameras. Other comparisons relate these measurements to LASCO observations[46]. It is this brightness calibration that is required to relate measurements of SMEI brightness to *in situ* densities measured around the Earth in the ambient and time-varying solar wind analyses from SMEI[44]. An error of this brightness calibration to 5% relates directly and in a linear way to an inaccurate 3D model determination of electron density for heliospheric structure. Besides giving ground truth for the dense structures we reconstruct in 3D in these analyses, the Ulysses *in situ* plasma observations help in these analyses as well to certify that the ratio of ambient to large (day-long) variable structures are not greatly different out of the ecliptic.

Even though the 3D reconstruction can be used when only SMEI's Thomson scattering brightness is available, better results are obtained when IPS velocity data (so far the only remote-sensing data to provide direct measurements of heliospheric solar wind speed) are included. The very best 3D reconstruction results are reached when SMEI photometric data are combined with IPS velocity data. Currently STELab provides IPS velocities in real-time most of the year, and these data are available for the SMEI data reduction as well as for study of the differences in the data sets.

These data sets can be compared with the LASCO and SECCHI observations and the results go a long way toward certifying the SMEI 3D data analyses. These analyses show which portions of CMEs observed in a coronagraph move outward into the interplanetary medium, They also show where individual features seen in the coronagraph images are present relative to the plane of the sky location usually assumed for coronagraph observations.

3. NEW SMEI RESULTS

Telemetry from SMEI is relayed from the ground stations to the AFRL SMEI data processing center, where data packets are concatenated, individual camera data frames are decompressed, and combined with an assigned set of spacecraft quaternions (spacecraft pointing derived from a star tracker). The resulting CCD data frames are placed on an AFRL FTP site at Sacramento Peak Observatory, and transferred to UCSD. UCSD maintains a database of these SMEI image frames in near real time on a local server. At the time of the SPIE meeting (August 26, 2007), these data frames have been reduced to sidereal sky maps to the UCSD SMEI photometric specification through day 160 (June 9) of year 2007 for all three SMEI cameras. Sacramento Peak Observatory also maintains an archive of original SMEI images. Figure 2a shows a set of simultaneous 4-second exposure "image frames" from these three cameras.

AFRL and UCSD have independently developed analysis sequences to reduce individual SMEI image frames whose final product is a heliospheric sky map for every orbit of data. Image frames from a complete orbit are combined into composite sky maps (as in Figure 2b, or Figures 3a and 3b) which are generally displayed with an angular resolution better than 1° at the orbital time cadence of 102 minutes. The AFRL analysis sequence uses similar steps to those at UCSD, but is specifically crafted to demonstrate the feasibility of detecting and tracking solar mass ejections in near real time. The AFRL analysis is focused on an expedient presentation of SMEI data in the form of 2D sky maps and these are presented in near real time on the National Solar Observatory website (**http://smei.nso.edu/**).

The UCSD SMEI analysis[2,47,48] is driven by the requirement that the SMEI sky maps approach as close as possible to full photometric and angular resolution design limits of SMEI. This enables the best quantitative analysis of the SMEI data. The promise of modeling heliospheric density structure using 3D reconstruction techniques is foremost here but requires careful accounting of the brightness from the instrument over a significant fraction of a 28-day solar rotation. This enables the study of slow (corotating) as well as rapidly moving transient features. Thus, sky maps must retain a constant temporal base over time periods of as many weeks as possible, to measure both corotating structures as well as fast-moving transient structures. The 3D reconstructions require optimal removal of non-heliospheric and zodiacal artifacts but also that as little as possible of the Thomson-scattered signal be inadvertently removed in the process.

Since light from the sidereal sky (stars, the Milky Way, nebulae, galaxies) is about 100× brighter than the variable Thomson-scattered signal, this background must be removed from orbit-to-orbit SMEI sky maps. The simplest way to do this is by subtracting one Sun-centered sky map from the next ("running differences"); here only the change in the heliospheric signal, due to motion of the structures, over the orbital time period (Δt = 102 minutes), remains. Tappin *et al.*[49] use this method to study the heliospheric response to the 28 May 2003 halo CME observed by SMEI on 29 May 2003. Several hundred transient events have been observed by this method in the SMEI observations to date[50], and more than half of these can be first identified as CMEs in the LASCO coronagraph data. Such difference maps are useful for real-time presentation of SMEI data, and adequate for identifying and even tracking disturbances distant from Earth. However, this simple analysis sacrifices the wealth of more slowly varying features present in SMEI data. This analysis also contains regions of positive and negative differences, complicating interpretation and a quantitative analysis.

Alternatively, a sidereal sky map averaged over many orbits close in time to a heliospheric event can be subtracted. This method preserves more heliospheric signal by effectively enlarging the base time scale Δt. Figures 3a and 3b show examples of such difference sky maps plotted in Sun-centered ecliptic coordinates for the 29 May 2003 CME event (see also Jackson *et al.*[2]) for two selected orbits.

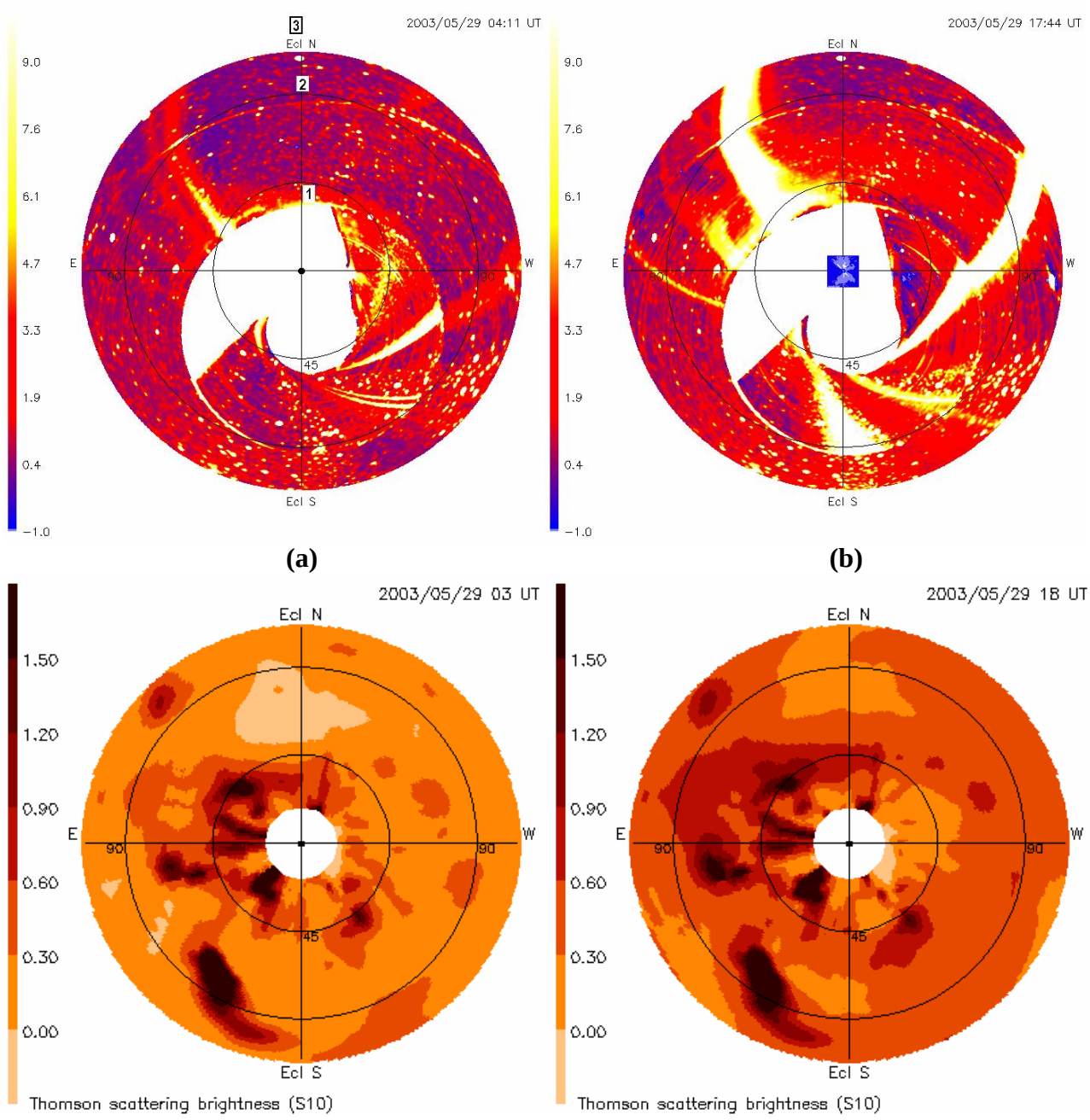

Figure 3. SMEI "fisheye" sky map images of the heliospheric response to the 28 May 2003 CME observed to "halo" the Sun in LASCO observations and in SMEI observed beyond 45° elongation in the first image set and to have begun to engulf the Earth at 90° elongation in the second at the times indicated. **(a)** and **(b)** Direct SMEI sky map images on 29 May 2003. Shown are two orbits of data differenced from an 8-orbit average for SMEI cameras 1, 2 and 3. The white regions in the sky maps that extend roughly outward from the center are primarily locations where auroral light is too bright to provide a photometric signal. The data were smoothed using a 1° Gaussian filter. The specks in each image are stellar signals – mostly bright stars that have changed brightness over the observation interval. Brightness is in SMEI camera analog to digital units (ADU). One S10 is approximately 0.4 ADU. A LASCO C3 coronagraph image is inserted in the top right map for scale. Numbered locations 1-3 on map **(a)** indicate the regions shown as time series in Figure 4. **(c)** and **(d)** The approximate same images showing far more features and the halo enhancement surrounding Earth are obtained from time series modeling as described later in the text using SMEI data from cameras 1, 2, and 3. Brightness is given in S10 normalized to an r^{-2} density falloff relative to the 90° elongation circle.

Our current analysis provides a stable baseline over several weeks, without sacrificing angular resolution. This provides a calibrated data set sufficient for the 3D analysis. The 3D results in turn refine SMEI images, and these can be presented from any desired viewing location; the original sky maps are often contaminated by troublesome backgrounds and portions of these are sometimes further swamped by bright auroral light. Extrapolating across these regions and removing contaminant signals is best accomplished as we do in IPS sky maps. Here, sky map outages and contaminant signals are handled by using a realistic 3D solar wind model iteratively fit to the data, both removing the contaminated regions and extrapolating across them. The best editing retains only the heliospheric signal in the sky maps. Figures 3c and 3d show samples of this technique's ability to refine 2D SMEI sky maps. Ultimately, the optimum removal of the sidereal and zodiacal sky map contributions rests on forming a long-term average of background zodiacal and stellar light over a large portion of a solar rotation together with individual-star subtraction for stars brighter than about 6th magnitude (Hick *et al.*[51]) in order to minimize the residual effects of bright stars on individual images and in the time series required to provide 3D reconstructions.

We show some of these data and analyses on a recent UCSD website (**http://smei.ucsd.edu/data.html** - see Figure 4). The website provides selected portions of the SMEI data set in all of these formats. Our intent is to populate this website as completely as possible over the next months. One innovation in this website is a comparison image-set containing both 3D-reconstructed SMEI sky maps and direct-image sky maps of the heliosphere similar to those shown in Figure 3. Both the 3D reconstructed sky maps and the direct sky maps contain noise from the various data processes used to provide them. Other analyses[40,43,45,52-54] use this and similar methods to relate remote sensing observations to densities measured *in situ*.

As an example, we have employed this technique to successfully analyze CME-associated structures using IPS and SMEI Thomson scattering observations for the 28 May 2003 halo CME event shown in Figure 3. Figure 5a, 5b, and 5c, are examples of the 3D heliospheric reconstruction analyses and imagery using SMEI Thomson scattering brightness and STELab IPS velocity data and digital time steps of ½ day, and resolutions in latitude and longitude of 6.7°. Gaussian filters are used for the two data sets and they limit the size of structures observed to larger than the digital resolution[43,44]. The density we reconstruct in Figure 5a clearly shows a great deal of structure in the ecliptic plane cut, and now that the STEREO spacecraft are more than a few degrees from the Sun-Earth line, we expect such structure to be well-documented in the STEREO *in situ* PLASTIC and IMPACT data. Figure 5d shows a preliminary comparison of our 3D model densities with the Advanced Composition Explorer (ACE) spacecraft plasma density data for this time interval and Figure 5e shows the correlation between the two.

SMEI cameras are calibrated using known G-star brightness[46] to an estimated 5% for all SMEI cameras (1 S10 = 0.46 ADU for SMEI camera 2). The time series obtained from the SMEI 3D reconstruction for the 28 May 2003 halo CME response currently produces a density peak at the same location in time as observed by the ACE and other spacecraft proton densities, and close in amplitude to the *in situ* result (Figure 5d). To compare more exactly to proton densities requires that a correction be included for heavier-element abundances throughout the remotely-observed CME structure,here assumed to add 25% more electrons, and thus 1 S10 = 0.60 ADU for the tomography comparison of *proton* density from SMEI white-light brightness observations.

Extrapolation of magnetic fields outward from the solar surface is currently done on a regular basis in order to forecast changes at the Earth to the inner planets and to the Ulysses spacecraft (see, for instance[55-59], and the UCSD website **http://ips.ucsd.edu/index_ss.html**). However, the most challenging measurements to remotely sense or extrapolate throughout the heliosphere are magnetic fields that are associated with coronal transients. These changing magnetic fields are responsible for many of the interactions present at planetary bodies, including Earth, but as yet a direct observation has proven difficult, because their primary change occurs in the solar corona, and so far, few observations exist to explore their transient effects. *In situ* magnetic field measurements for certain assumed structures (flux ropes) can be reconstructed, and these compared with the density and velocity 3D reconstructions. Figure 6 shows one such example from the analysis of the 28 October 2003 halo CME[44] as given in several journal articles and presentations[60-62].

An alternative approach to obtain heliospheric magnetic field measurements involves Faraday Rotation (FR) from ground-based techniques and either coronal sounding measurements from interplanetary spacecraft[63-69] or natural-occurring radio sources[70-73]. However, it is uncertain how well these observations can be analyzed to obtain an FR signal over large elongations from the Sun because of the low polarizations of these radio sources and the considerable noise present from ionospheric variations at low radio frequencies.

SMEI Fisheye Sky Maps

Archive by Day (Explanation)

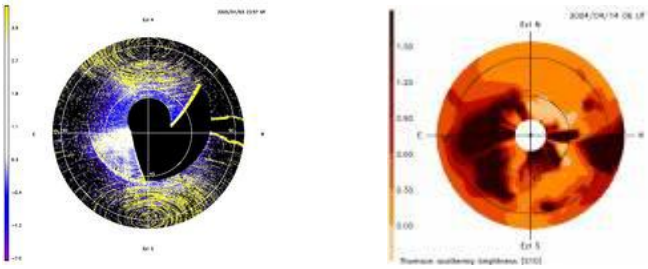

(Comparison)

Direct Difference Reconstructed

SMEI Hammer-Aitoff Sky Maps

Archive by Day (Explanation)

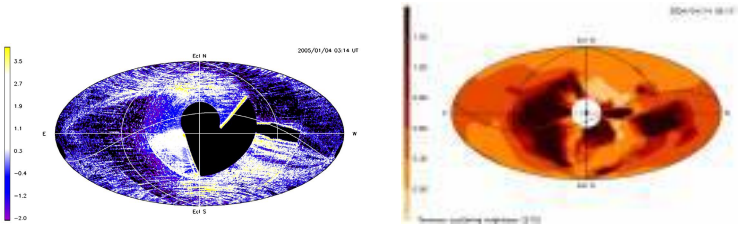

(Comparison)

SMEI 3D Reconstructions

Archive by Day (Explanation)

nv3_files

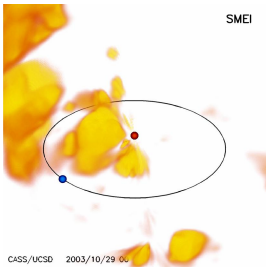

Timeseries

Vox Files

45º West of Sun-Earth

SMEI Sky Map Archive

Archive

(Explanation)

Original FITS

Processed GRD Files

Data Set

SMEI Image Frames

(Explanation)

Archive

Figure 4. Proposed UCSD website front page giving the data products available for the UCSD SMEI server (**http://smei.ucsd.edu/**). The data set provides direct long term background subtracted and orbit difference images in two formats, Fisheye and Hammer-Aitoff, the 3D reconstructed images in the same format, and a comparison of these direct and reconstructed images. In addition, a remotely observed view of the images will be provided from given perspective. The announcement of other data products are shown, and will be available on a "by request" basis from UCSD.

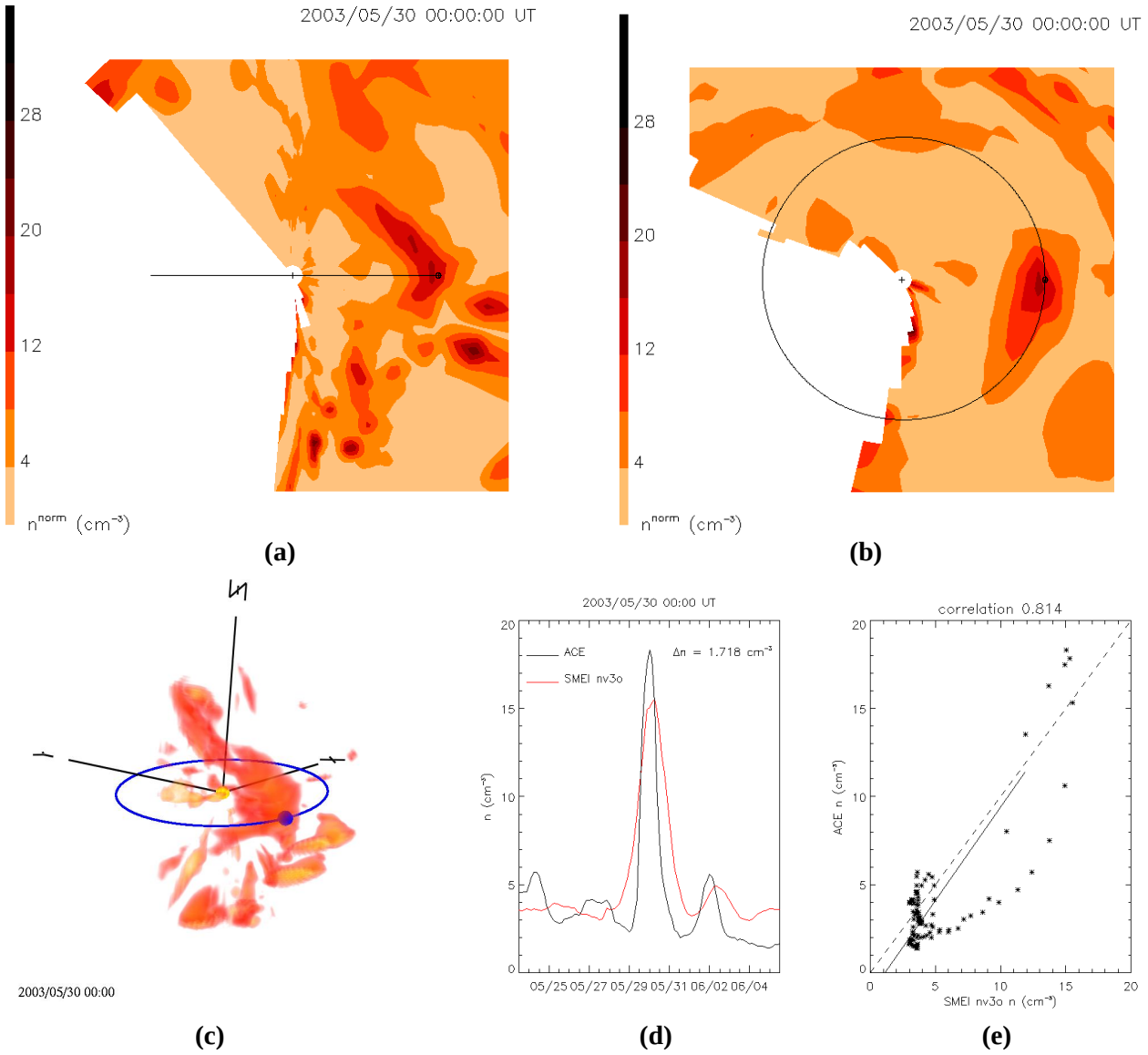

Figure 5. Reconstruction of the 28 May 2003 Halo CME as it is about to hit Earth using both SMEI brightness and IPS velocity data. 3D density reconstruction of the 28 May halo CME as it reaches Earth. Earth orbit is shown as a black line in the image in (a) and (b) and a blue ellipse in (c), with the Earth as a black dot in (a) and (b), blue in (c). To the left of each image in (a) and (b) is the density scale. An r^{-2} density fall-off has been removed from the analysis to better show structures at different radii relative to the nominal density at ~1 AU. The digital angular resolution is 6.7° × 6.7° in latitude and longitude. The 3D reconstructions have a digital temporal cadence of ½ day. The blank region to the left in each reconstruction is the location unavailable to the SMEI reconstructions. The density enhancement of the CME hitting Earth is a relatively small feature compared with the overall CME structure leaving the Sun **(a)** Density in a meridian-plane cut from East of the Sun-Earth line. **(b)** Density in an ecliptic-plane cut from East of the Sun-Earth line. The CME that hits Earth in this event is more extensive to the East of the Sun. **(c)** Density as seen from 1.5 AU, ~20° above the ecliptic ~30º East of the Sun-Earth line at 00:00 UT. The main structure near Earth is associated with the halo CME observed by LASCO on 28 May 2003. **(d)** Time series plot of the density at Earth extracted from the reconstruction in comparison with ACE observations. ACE observations are combined into 12-hour averages matching the temporal and spatial resolutions of the SMEI 3D brightness reconstruction. The correlation has been limited to data times within about 5 days of the event. **e)** Correlation of the 3D reconstructed model with ACE 12-hour averaged data.

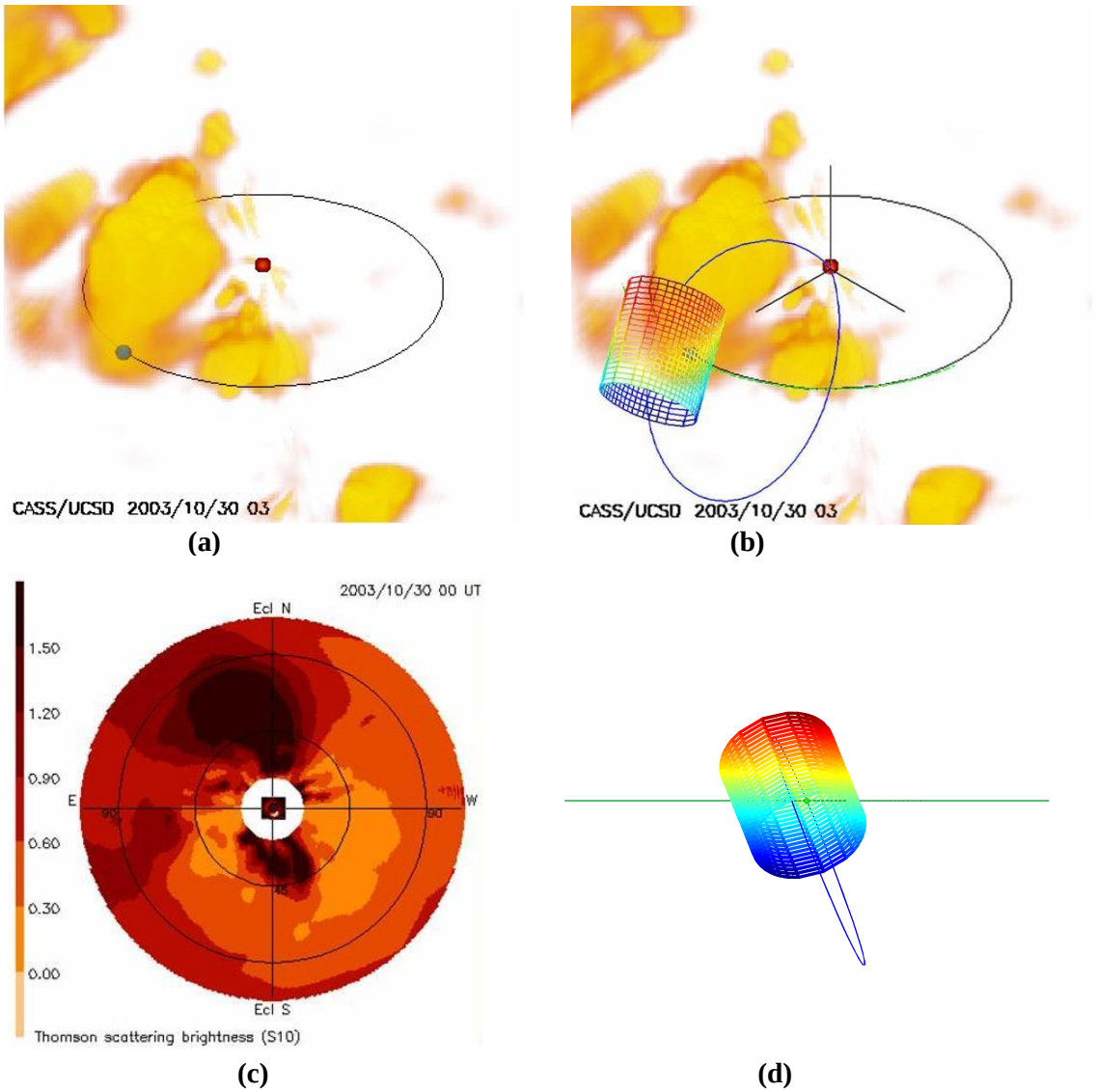

Figure 6. (a) Density reconstruction of the heliospheric response to the 28 October 2003 CME viewed from 3.0 AU 30º above the ecliptic plane and 45º West of the Sun-Earth line. The Earth is indicated as a blue circle in its elliptical orbit. The Sun is indicated by a red circle. Contours are from 10 e^{-} cm^{-3} to 30 e^{-} cm^{-3} and have an r^{-2} density gradient removed. A portion of the ejecta associated with a solar prominence is observed to the South of the Sun in this view[59-61]. **(b)** Same as (a) with reconstructed flux rope cylinder from ACE superposed. **(c)** 2D map of the heliosphere as viewed from Earth. The 28 October 2003 image of the CME from the LASCO C2 coronagraph at 1106 UT is superposed at the center at its appropriate size. **(d)** The flux rope cylinder viewed from behind the Earth looking directly towards the Sun without perspective. The horizontal line marks the ecliptic and is drawn to a total length of 2.0 AU.

4. CONCLUSION

The Solar Mass Ejection Imager (SMEI) continues to operate successfully after more than four years. The present article details how we determine the extent of several CME events in SMEI observations (including those of 28 May 2003 and 28 October 2003). We are able to measure these events from their first observations as close as 20° from the solar disk until they fade away in the SMEI ~180° field of view. 3D reconstruction techniques provide perspective views from outward-flowing solar wind as observed from Earth. This 3D modeling technique enables separating the true heliospheric response in SMEI from background noise, and reconstructing the 3D heliospheric structure as a function of time.

Although these reconstructions allow separation of the 28 October 2003 CME from other nearby heliospheric structure, they are preliminary in that they use only approximately 1/25th of the total available lines of sight from SMEI. In addition, the reconstructions are limited by aurora and other sources of noise present in the SMEI data sets that is removed as carefully as possible to provide the best reconstructions. To utilize more lines of sight (that will allow a many-fold enhancement of the 3D reconstructions) will require significantly more computer resources than are now allocated to the reconstruction process, and the careful elimination of the effects of brighter stars in SMEI sky maps.

ACKNOWLEDGEMENTS

This work was supported in part by contract NSF grant ATM-0331513, NASA grant NNG05GM58G, and NASA subcontract #0673-1 through Boston College, as well as contract FA8718-04-C-0050 from the U.S. Air Force. We are extremely grateful to M. Kojima, M. Tokumaru, and the staff at STELab, Japan, who have made IPS data available to UCSD under the auspices of a joint collaborative agreement between the Center for Astrophysics and Space Sciences (CASS), UCSD, and STELab. This work would not have been possible without the support of T. Kuchar, D. Mizuno, S. Price, and D. Sinclair, of the Air Force Research Laboratory, Hanscom AFB, who organized and have distributed the SMEI data to team members. In addition, we acknowledge the continuing support of D. Webb. SMEI was designed and constructed by a team of scientists and engineers from the U.S. Air Force Research Laboratory, the University of California at San Diego, Boston College, Boston University, and the University of Birmingham in the U.K. Financial support was provided by the Air Force, the University of Birmingham, and NASA. We would also like to extend particular thanks to UCSD student J. M. Clover for help in the SMEI analyses and website design, and to the ACE|SWE group for use of their data in this paper for *in situ* comparisons. SOHO|LASCO data are used courtesy of the LASCO consortium. The SOHO mission is a joint programme of ESA and NASA.

REFERENCES

1. C.J. Eyles, G.M. Simnett, M.P. Cooke, B.V. Jackson, A. Buffington, P.P. Hick, N.R. Waltham, J.M. King, P.A. Anderson, and P.E. Holladay, The Solar Mass Ejection Imager (SMEI), *Solar Phys.*, **217**, 319, 2003.
2. B.V. Jackson, A. Buffington, P.P. Hick, R.C. Altrock, S. Figueroa, P.E. Holladay, J.C. Johnston, S.W. Kahler, J.B. Mozer, S. Price, R.R. Radick, R. Sagalyn, D. Sinclair, .G.M. Simnett, C.J. Eyles, M.P. Cooke, S.J. Tappin, T. Kuchar, D. Mizuno, D.F. Webb, P.A. Anderson, S.L. Keil, R.E. Gold, and N.R. Waltham, The Solar Mass Ejection Imager (SMEI) Mission, *Solar Phys.* **225**, 177, 2004.
3. A. Buffington, D.L. Band, B.V. Jackson, P.P. Hick, and A.C. Smith, A Search for Early Optical Emission at Gamma-Ray Burst Locations by the Solar Mass Ejection Imager (SMEI), *Astrophys. J*. **637**, 880-888, 2006.
4. B.V. Jackson, H.S. Hudson, J.D. Nichols, and R.E. Gold, Design Considerations for a "Solar Mass Ejection Imager" on a Rotating Spacecraft, in *Solar System Plasma Physics Geophysical Monograph*, **54**, J.H. Waite, Jr., J.L. Burch and R.L. Moore, eds., 291, 1989.
5. B. Jackson, R. Gold, and R. Altrock, R., The Solar Mass Ejection Imager, *Adv. in Space Res*., **11**, 377, 1991.
6. B.V. Jackson, A. Buffington, P.L. Hick, S.W. Kahler, R.C. Altrock, R.E. Gold R.E., and D.F. Webb, The Solar Mass Ejection Imager, in *Solar Wind Eight*, D. Winterhalter, J.T. Gosling, S.R. Habbal, W.S. Kurth and M. Neugebauer, eds., AIP Conference Proceedings **382**, Woodbury, 536, 1995.
7. B.V. Jackson, A. Buffington, P.L. Hick, S.W. Kahler, G. Simnett, and D.F. Webb, The solar mass ejection imager, *Physics and Chemistry of the Earth*, **22**, No. 5, 441, 1997.
8. S.L. Keil, R.C. Altrock, S.W. Kahler, B.V. Jackson, A. Buffington, P.L. Hick, G. Simnett, C. Eyles, D.F. Webb, and P. Anderson, The Solar Mass Ejection Imager (SMEI), Denver 96 "Missions to The Sun", *SPIE* **2804**, 78, 1996.
9. M. Kaiser, The STEREO Mission: and Overview, *Adv. Space Res*., **36(8)**, 1483-1488, 2005.
10. L.M. Blush, F. Allegrini, P. Bochsler, H. Daoudi, A. Galvin, R. Karrer, L. Kistler, B. Klecker, E. Mobius, A. Optiz, M. Popecki, B. Thompson, R.F. Wimmer-Schweingruber, and P. Wurz, Development and calibration of major components for the STEREO/Plastic (plasma and suprathermal ion composition) instrument, *Adv. Space Res*., **36(8)**, 1544-1556, 2005.
11. J.G. Luhmann, D.W. Curtis, R.P. Lin, D. Larson, P. Schroeder, A. Cummings, R.A. Mewaldt, E.C. Stone, A. Davis, T. von Rosenvinge, M.H. Acuna, D. Reames, C. Ng, K. Ogilvie, R. Mueller-Mellin, H. Kunow, G. M.

Mason, M. Wiedenbeck, A. Sauvaud, C. Aoustin, P. Louarn, J. Dandouras, A. Korth, V. Bothmer, V. Vasyliunas, T. Sanderson, R.G. Marsden, C.T. Russell, J.T. Gosling, J.L. Bougeret, D.J McComas, J.A Linker, P. Riley, D. Odstrcil, V.J. Pizzo, T. Gombosi, D. DeZeeuw, and K. Kecskemety, IMPACT: Science Goals and firsts with STEREO, *Adv. Space Res.*, **36(8)**, 1534-1543, 2005.

12. W.T. Thompson, J.M., Davila, R.R. Fisher, L.E. Orwig, J.E. Mentzell, S.E. Hetherington, R.J. Derro, R.E. Federline, D.C. Clark, P.T. Chen, J.L. Tveekrem, A.J. Martino, J. Novello, R.P. Wesenberg, O.C. St. Cyr, N.L. Reginald, R.A. Howard, K.I. Mehalick, M.J. Hersh, M.D. Newman, D.L. Thomas, G.C. Card, D. Elmore, COR1 inner coronagraph for STEREO-SECCHI, in *Proc. SPIE* **4853,** 1-11, 2003.
13. R.A. Harrison, C.J. Davis and C.J. Eyles, The STEREO Heliospheric Imager: How to Detect CMEs in the Heliosphere, *Adv. Space Res.*, **36(8)**, 1512-1523, 2005.
14. C.J. Davis and R.A. Harrison, STEREO/HI – from near-Earth objects to 3D comets, *Adv. Space Res.*, **36(8)**, 1524-1529, 2005.
15. K.-P. Wenzel, R.G Marsden, D.E. Page, and E.J. Smith, The Ulysses Mission, *Astron. Astrophys. Suppl. Ser.*, **92**, 267, 1992.
16. S.J. Bame, D.J. McComas, B.L. Barraclough, J.L. Phillips, K.J. Sofaly, J.C. Chavez, B.E. Goldstein, and R.K. Sakuri, The ULYSSES solar wind plasma experiment, *Astron. Astrophys. Suppl. Ser.*, **92**, 237, 1992.
17. A. Balogh, T.J. Beek, *et al.*, The magnetic field investigation on the ULYSSES mission – Instrumentation and preliminary scientific results, *Astron. Astrophys. Suppl. Ser.*, **92**, 221, 1992.
18. L. Biermann, Cometenschweifen und solare korpuskularstrahlung, *Zs. F. Astrophys.*, **29**, 274–286, 1951.
19. A. Hewish, P.F. Scott, D. and Wills, Interplanetary scintillation of small diameter radio sources, *Nature*, **203**, 1214, 1964.
20. Z. Houminer, Corotating plasma streams revealed by interplanetary scintillation, *Nature Phys. Sci.***, 231**, 165, 1971.
21. S. Ananthakrishnan, W.A. Coles, J.J. and Kaufman, Microturbulence in solar wind streams, *J. Geophys. Res.*, **85**, 6025, 1980.
22. W.A. Coles, B.J. Rickett, V.H. Rumsey, J.J. Kaufman, D.G. Turley, S. Ananthakrishnan, J.W. Armstrong,, J.K. Harmon, S.L. Scott, and D.G. Sime, *Nature* **286**, 239, 1980.
23. A. Hewish, and S. Bravo, The sources of large-scale heliospheric disturbances, *Solar Phys.*, **106**, 185, 1986.
24. K.W. Behannon, L.F. Burlaga, and A. Hewish, Structure and evolution of compound streams at ≤1 AU, *J. Geophys. Res.*, **96**, 21, 213, 1991.
25. M. Kojima, and T. Kakinuma, Solar Cycle Evolution of Solar Wind Speed Structure between 1973 and 1985 Observed with the Interplanetary Scintillation Method, *J. Geophys. Res.* **92**, 7269, 1987.
26. P. Hick, B.V. Jackson, R. and Schwenn, Synoptic Maps for the Heliospheric Thomson Scattering Brightness as Observed by the Helios Photometers, *Astron. Astrophys*. **285**, 1, 1990.
27. D.C. Wilson, *NCAR Cooperative Thesis No. 40*, Ph.D. thesis to the University of Colorado, Boulder, Colorado, 1977.
28. B.V. Jackson, A coronal hole equatorial extension and its relation to a high speed solar wind stream, *Topical Conference on Solar and Interplanetary Physics*, Tucson, Arizona,. 7, 12-15 January, 1977.
29. N.E. Hurlburt, P.C.H. Martens, and G.L. Slater, Volume reconstruction of magnetic fields using solar imagery, *ASP Conf. Series*, **68**, 30, 1994.
30. S. Zidowitz, Coronal structure of the Whole Sun Month: A tomographic reconstruction, *J. Geophys Res.*, **104**, **A5**, 9727-9734, 1999.
31. A.V. Panasyuk, Three-dimensional reconstruction of UV emissivities in the solar corona using Ultraviolet Coronagraph Spectrometer data from the Whole Sun Month, *J. Geophys. Res.*, **104**, 9721, 1999.
32. R.A. Frazin, Tomography of the solar corona. I. A robust, regularized, positive estimation method, *Astrophys. J.*, **530**, 1026, 2000.
33. R.A. Frazin, and P. Janzen, Tomography of the solar corona. II. Robust, regularized, positive estimation of the three-dimensional electron density distribution from LASCO-C2 polarized white-light images, *Astrophys. J.*, **570**, 408, 2002.
34. K.W. Behannon, L.F. Burlaga, and A. Hewish, Structure and evolution of compound streams at ≤ 1 AU, *J. Geophys. Res.*, **96**, 21, 213, 1991.
35. B.V. Jackson, P.L. Hick, M. Kojima, and A. Yokobe, Heliospheric tomography using interplanetary scintillation observations, *Physics and Chemistry of the Earth*, **22**, No. 5, 425, 1997.

36. B.V. Jackson, P.L. Hick, M. Kojima, and A. Yokobe, Heliospheric Tomography Using Interplanetary Scintillation Observations, for the COSPAR XXXI meeting held in Birmingham, England 14-21 July, 1996 *Adv. in Space Res.*, **20**, No. 1, 23, 1997.
37. B.V. Jackson, P.L. Hick, M. Kojima, and A. Yokobe, Heliospheric Tomography Using Interplanetary Scintillation Observations 1. Combined Nagoya and Cambridge data, *J. Geophys. Res*., **103**, 12,049, 1998.
38. M. Kojima, M., Tokumaru, H. Watanabe, A. Yokobe, A., Asai, K., Jackson, B.V. and Hick, P.L., 1998, Heliospheric Tomography Using Interplanetary Scintillation Observations 2. Latitude and Heliocentric Distance Dependence of Solar Wind Structure at 0.1-1 AU, *J. Geophys. Res*., **103**, 1981.
39. B.V. Jackson, and P.P. Hick, Corotational tomography of heliospheric features using global Thomson scattering data, *Solar Phys*., **211**, 344, 2002.
40. B.V. Jackson, A. Buffington, and P.P. Hick, A heliospheric imager for solar orbiter, Proc. of "Solar Encounter: The First Solar Orbiter Workshop", Puerto de la Cruz, Tenerife, Spain, 14-18 May 2001 (*ESA* **SP-493**, September 2001), 251, 2001.
41. B.V. Jackson, P.P. Hick, and A. Buffington, Time-dependent tomography of heliospheric features using the three-dimensional reconstruction techniques developed for the Solar Mass Ejection Imager (SMEI), *Proc. SPIE, Waikoloa*, 22-28 August 2002, **4853**, 23, 2002.
42. B.V. Jackson , P.P. Hick and A. Buffington, Time-dependent tomography of heliospheric features using interplanetary scintillation (IPS) remote-sensing observations, *Proceedings of Solar Wind 10*, Pisa, June 17-21, 75, 2003.
43. B.V. Jackson, and P.P. Hick, Three-dimensional tomography of interplanetary disturbances, in: Solar and Space Weather Radiophysics Current Status and Future Developments, D.G. Gary and C.U. Keller, eds., *ASSL* **314**, Kluwer, The Netherlands, 355, 2004.
44. B.V. Jackson, A. Buffington, P.P Hick, X. Wang, and D. Webb, Preliminary three-dimensional analysis of the heliospheric response to the 28 October 2003 CME using SMEI white-light observations, *J. Geophys. Res.* **111, A4**, A04S91, 2006.
45. B.V. Jackson, J.A. Boyer, P.P. Hick, A. Buffington, M.M. Bisi, and D.H. Crider, Analysis of Solar Wind Events Using Interplanetary Scintillation (IPS) Remote Sensing 3D Reconstructions and Their Comparison at Mars, *Solar Phys*., 241, 385-396, 2007.
46. A. Buffington, J.S. Morrill, P.P. Hick, R.A. Howard, B.V. Jackson, and D.F. Webb, Analysis of the Comparative Responses of SMEI and LASCO, in *Proc. SPIE* **6689**, 2007 (submitted),
47. P.P. Hick, A. Buffington, and B.V. Jackson,, The SMEI real-time data pipeline: From raw CCD frames to photometrically accurate full-sky maps, *Proc. of SPIE*, 59011B, doi: 10.1117/12.617996, 2005.
48. P.P Hick, A. Buffington, and B.V. Jackson, 2006, The UCSD/SMEI Data Processing Pipeline, SHINE 06 Workshop, Midway, UT, 31 July - 4 August, 2006.
49. S.J. Tappin, A. Buffington, M.P. Cooke, C.J. Eyles, P.P. Hick, P.E. Holladay, B.V. Jackson, J.C. Johnston, T. Kuchar, D. Mizuno, J.B. Mozer, S. Price, R.R. Radick, G.M. Simnett, D. Sinclair, N.R. Waltham, and D.F. Webb, Tracking a Major Interplanetary Disturbance with SMEI, *Geophys. Res. Lett.* , **31**, 2802, 2004.
50. D.F. Webb, D.R. Mizuno, A Buffington, M.P. Cooke, C.J. Eyles, C.D. Fry, L.C. Gentile, P.P. Hick, P.E. Holladay, T.A. Howard, J.G. Hewitt, B.V. Jackson, J.C. Johnston, T.A. Kuchar, J.B. Mozer, S. Price, R.R. Radick, G.M. Simnett, and S.J. Tappin, Solar Mass Ejection Imager (SMEI) Observations of CMEs in the Heliosphere, *J. Geophys. Res.*, **111**, A12101, doi:10.1029/2006JA011655, 2006.
51. P.P. Hick, A. Buffington, and B.V. Jackson, A Procedure for Fitting Point Sources in SMEI White-Light Full-Sky Maps, in *Proc. SPIE* **6689**, 2007 (submitted).
52. B.V. Jackson, P.P. Hick, and A. Buffington, The 20 January 2005 CME Solar Mass Ejection Imager (SMEI) Analyses, *EOS Trans. AGU* 87(52), Fall Meet. Suppl., Abstract SH33A-0396, 2006.
53. B.V. Jackson, P.P. Hick, A. Buffington, M.M. Bisi, and E.A. Jensen, Solar Mass Ejection Imager (SMEI) Analysis of the 20 January 2005 CME, SHINE 07 Workshop, Whistler, Canada, 30 July - 3 August, 2007.
54. M.M. Bisi, B.V. Jackson, P.P. Hick, A. Buffington, J.M. Clover, 3D Reconstructions of the Early November 2004 CDAW Geomagnetic Storms: Preliminary analysis of STELab IPS speed and SMEI density, *Geophys Res Letts*., 2007 (submitted).
55. T Dunn, B.V. Jackson, P.P. Hick and A. Buffington, Forecasting solar wind parameters using IPS tomography, *EOS Trans. AGU*, **80**, F790, 1999.
56. T. Dunn, B.V. Jackson, P.P. Hick and A. Buffington, Introduction of the CSSS magnetic field model into the UCSD tomographic solar wind model, *EOS Trans. AGU*, **82 (47)**, Fall Meet. Suppl., Abstract SH31A-0701, 2001.

57. T. Dunn, B.V. Jackson, P.P. Hick and A. Buffington, Introduction of the CSSS Magnetic Field Calculation into the UCSD Tomographic Solar Wind Model, at the SEC Space Weather Week, at the SEC Space Weather Week, April 16-19, Boulder, Colorado, 2002.
58. T.J. Dunn, P.P. Hick, B.V. Jackson, and X. Zhao, Inclusion of the CSSS magnetic field calculation into the UCSD tomographic solar wind model, *Proc. SPIE, Waikoloa*, 22-28 August 2002, **4853**, 504, 2002.
59. T. Dunn, B.V. Jackson, P.P. Hick, A. Buffington, and X.P. Zhao, Comparative Analyses of the CSSS Calculation in the UCSD Tomographic Solar Observations, *Solar Phys.* **227**, 339-353, 2005.
60. E.A. Jensen, T. Mulligan, B.V. Jackson, and M. Tokumaru, 3-D Magnetic Field Geometry of the October 28, 2003 ICME: Comparison with SMEI White-Light Observations, *EOS Trans. AGU* **87(52)**, Fall Meet. Suppl., Abstract SH33A-0397, 2006.
61. B.V. Jackson, P.P. Hick, A. Buffington, M.M. Bisi, M. Kojima, and M. Tokumaru, Comparison of the extent and mass of CME events in the interplanetary medium using IPS and SMEI Thomson scattering observations, Proceedings of the International Colloquium on Scattering and Scintillation in *Astronomical and Astrophysical Transactions*, I. Chashei and V. Shishov, eds., 2007 (in press).
62. T. Mulligan, E.A. Jensen, and B.V. Jackson, Magnetic flux rope model geometry constraints and their relationship to the SMEI 3D density reconstruction analyses for the October 29, 2003 ICME, *Geophys. Res. Letts*., 2007 (submitted).
63. M.K. Bird, H. Volland, R.A. Howard, M.J. Koomen, D.J. Michels, N.R. Sheeley, Jr., J.W. Armstrong, B.L. Seidel, C.T. Stelzried, and R. Woo, White-Light and Radio Sounding Observations of Coronal Transients, *Solar Phys.*, **98**, 341, 1985.
64. M.K. Bird, and P. Edenhofer, Remote sensing observations of the solar corona, in: R. Schwenn, and E. Marsch (eds.), Physics of the Inner Heliosphere I, Springer-Verlag, Berlin, pp. 13–97, 1990.
65. E.A. Jensen, High Frequency Faraday Rotation Observations of the Solar Corona, PhD Dissertation, Department of Earth and Space Sciences, UCLA, 2007.
66. E.A. Jensen, and C.T. Russell, Faraday rotation observations of flux ropes, MHD waves, and the large scale coronal magnetic field, presentation at IAGA, 2 – 13 July, 2007, Perugia, Italy, 2007.
67. E.A. Jensen and C.T. Russell, Measuring the plane of polarization in a strongly circular signal, in *Proc. SPIE* **6689**, 2007 (submitted).
68. E.A. Jensen, M.K. Bird, M. Paetzold, S.W. Asmar, J.D. Anderson, L. Iess, and C.T. Russell, The Cassini Solar Conjunction Faraday Rotation Experiment, *Adv. In Space Res.* 36, 1587-1594, 2005.
69. E.A. Jensen, J. Luhmann, and C. Russell, Faraday Rotation Observations and the PFSS Model, CMEs and Alfven Waves, SHINE 06 Workshop, Midway, UT, 31 July - 4 August, 2006.
70. M.K. Bird, E. Schrufer, H. Volland, W. Sieber, Coronal Faraday rotation during solar occultation of PSR 0525+21, *Nature*, **283**, 459-460, 1980.
71. S. Mancuso, and S.R. Spangler, Coronal Faraday Rotation Observations: Measurements and Limits on Plasma Inhomogeneities, *Astrophys. J.*, **525**, 195, 1999.
72. S. Mancuso, and S.R. Spangler, Faraday Rotation and Models for the Plasma Structure of the Solar Corona, *Astrophys. J.*, **539**, 480, 2000.
73. J.E. Salah, C.J. Lonsdale, D. Oberoi, R.J. Capallo, and J.C. Kasper, Space weather capabilities of low frequency radio arrays, *Proc. SPIE*, **5901**, 59010G-1, 2005.

---

* bvjackson@ucsd.edu; phone 1 858 534-3358; fax 1 858 534-0177; http://casswww.ucsd.edu/solar/smei/index.html; mail code 0424, UCSD, 9500 Gilman Drive, La Jolla, CA 92093-0424
** abuffington@ucsd.edu; phone 1 858-534-6630; fax 1 858 534-7051;
*** pphick@ucsd.edu; phone 1 858 534-8965; fax 1 858 534-0177
**** mmbisi@ucsd.edu; 1 858 534-0179; fax 1 858 534-0177
***** ejensen@ucsd.edu; 1 858 534-0179; fax 1 858 534-0177